

Supplementary information

**Multi-scale characterization of submicronic  
NASICON-type solid electrolyte  
 $\text{Li}_{1.3}\text{Al}_{0.3}\text{Ti}_{1.7}(\text{PO}_4)_3$  degraded by spark  
plasma sintering**

Gwenaëlle Courbaron <sup>a,b</sup>, Rafaël Bianchini-Nuernberg <sup>a\*</sup>, Jon Serrano Sevillano <sup>a,d,e</sup>, U-Chan Chung <sup>a</sup>,  
Mathieu Duttine <sup>a</sup>, Christine Labrugère-Sarroste <sup>f</sup>, Jacob Olchowka <sup>a,c,d</sup>, Dany Carlier <sup>a,c,d</sup>,  
Nathalie Delpuech <sup>b,c,d</sup> and Laurence Croguennec <sup>a,c,d\*</sup>

<sup>a</sup> Univ. Bordeaux, CNRS, Bordeaux INP, ICMCB, UMR 5026, F-33600 Pessac, France

<sup>b</sup> Renault SAS, Technocentre, 1 avenue du golf, 78280 Guyancourt, France

<sup>c</sup> RS2E, Réseau Français sur le Stockage Electrochimique de l'Energie, FR CNRS 3459,  
France

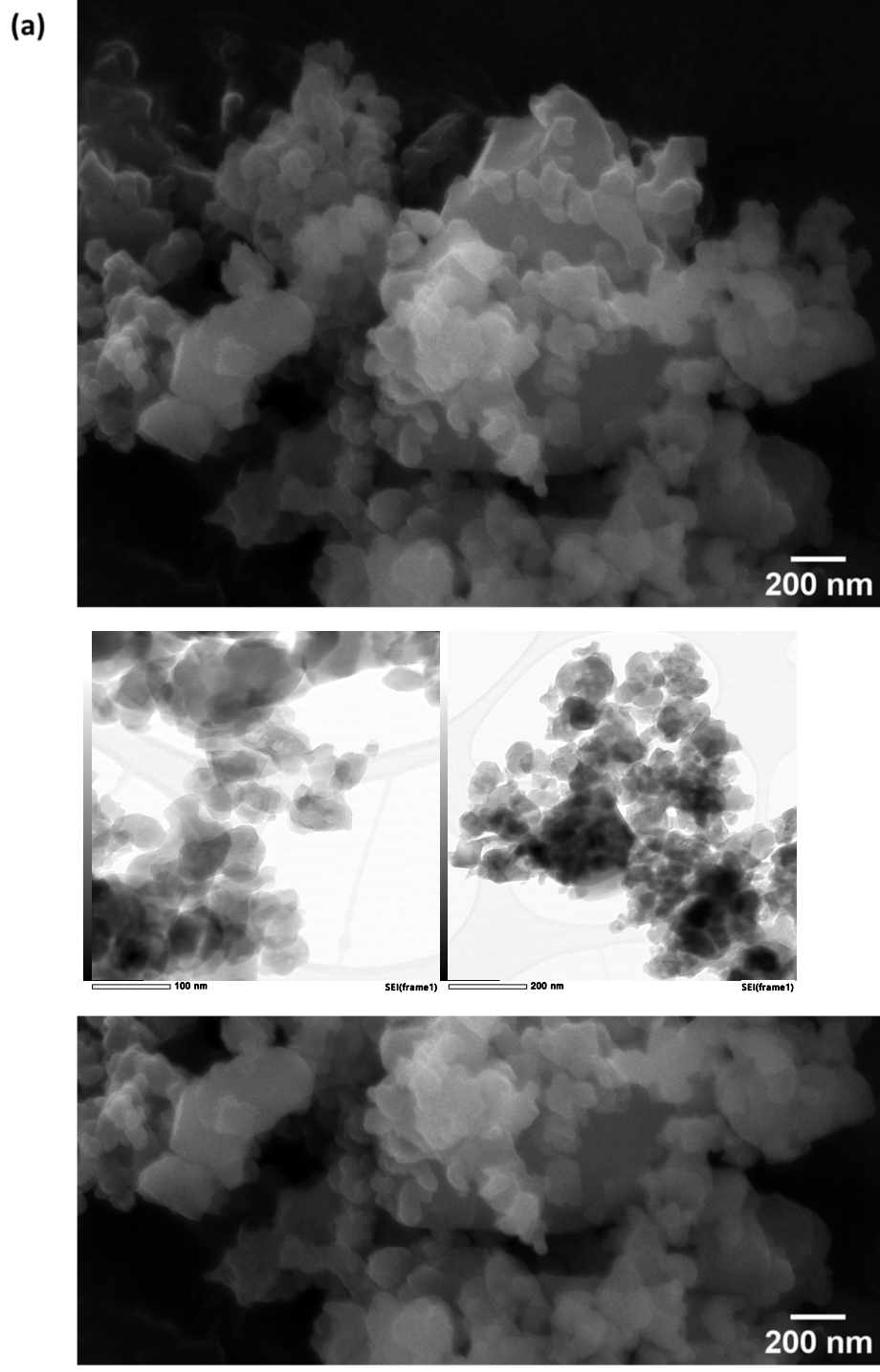
<sup>d</sup> ALISTORE-ERI European Research Institute, FR CNRS 3104, 80039 Amiens Cedex  
France

<sup>e</sup> CIC Energigune, Albert Einstein 48, Parque Tecnológico de Alava, Miñano 01510, Spain

<sup>f</sup> PLACAMAT, UAR 3626, CNRS Université Bordeaux, 33600 Pessac, France

\* corresponding authors: Laurence Croguennec ([laurence.croguennec@icmcb.cnrs.fr](mailto:laurence.croguennec@icmcb.cnrs.fr)) and  
Rafaël Bianchini-Nuernberg ([rafael.bianchini-nuernberg@icmcb.cnrs.fr](mailto:rafael.bianchini-nuernberg@icmcb.cnrs.fr))





(b)

<i>Element</i>	<i>Atomic ratio</i>	<i>Nominal composition</i>	<i>Deviation (%)</i>
----------------	---------------------	----------------------------	----------------------

Figure S1: SEM and TEM images of primary submicronic particles of commercial LATP powder (a) ; results of ICP-OES chemical analyses performed for this LATP powder and their comparison with the expected nominal composition (b)

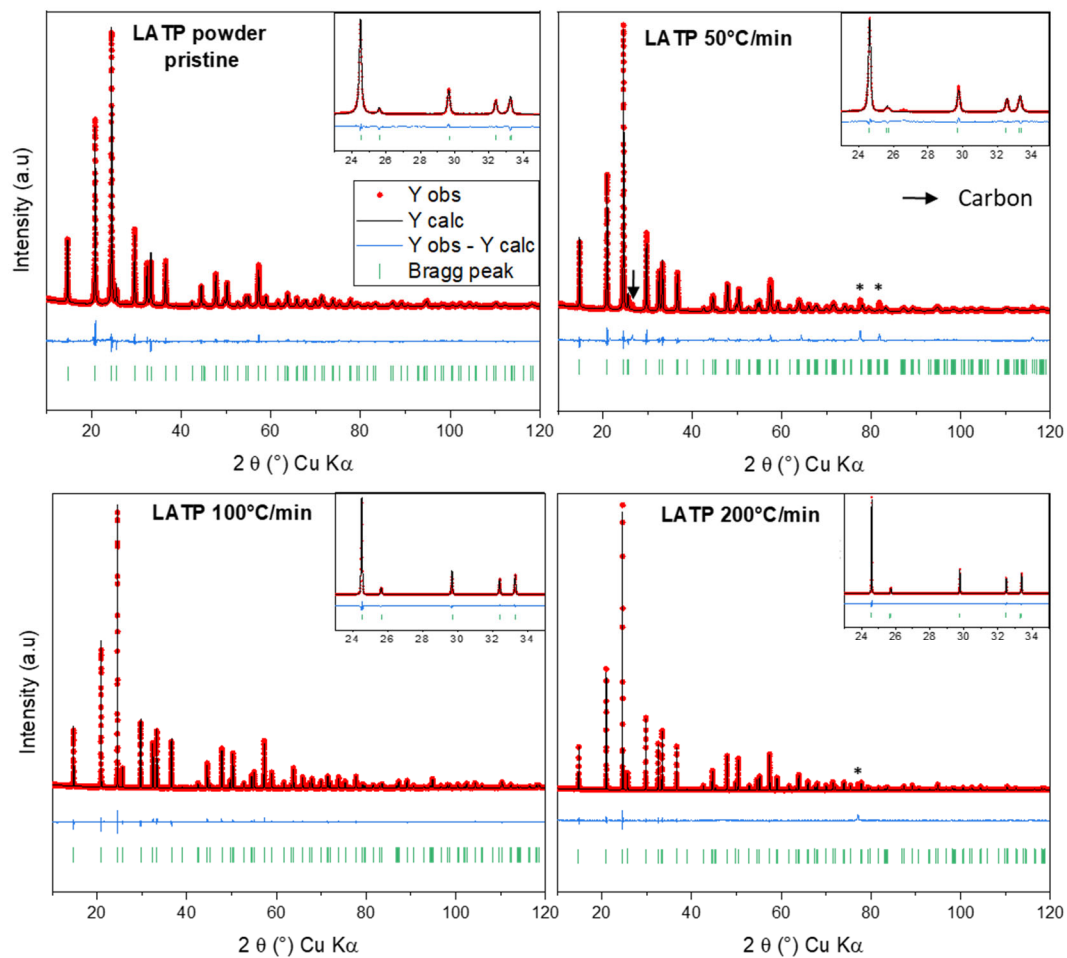


Figure S2: Rietveld refinements obtained for the pristine LATP powder and for the samples sintered by SPS at heating rates of 50°C/min, 100°C/min and 200°C/min

Table S1: Lattice parameters and cell volume determined by Rietveld refinement of XRD patterns

<b>Sample</b>	<b>a (Å)</b>	<b>c (Å)</b>	<b>V (Å<sup>3</sup>)</b>
<b><i>Pristine</i></b>	8.505(2)	20.845(5)	1305.8(6)
<b><i>LATP 50 °C/min</i></b>	8.481(3)	20.884(9)	1300 (1)
<b><i>LATP 73 °C/min</i></b>	8.4987(2)	20.8005(8)	1301.10(5)
<b><i>LATP 100 °C/min</i></b>	8.5028(3)	20.8048(7)	1302.61(8)
<b><i>LATP 200 °C/min</i></b>	8.4988(4)	20.794(1)	1300.7(1)
<b><i>LATP 300 °C/min</i></b>	8.4996(2)	20.7990(8)	1301.28(5)
<b><i>LATP CS 800°C, 5h</i></b>	8.5006(2)	20.8030(8)	1301.83(5)

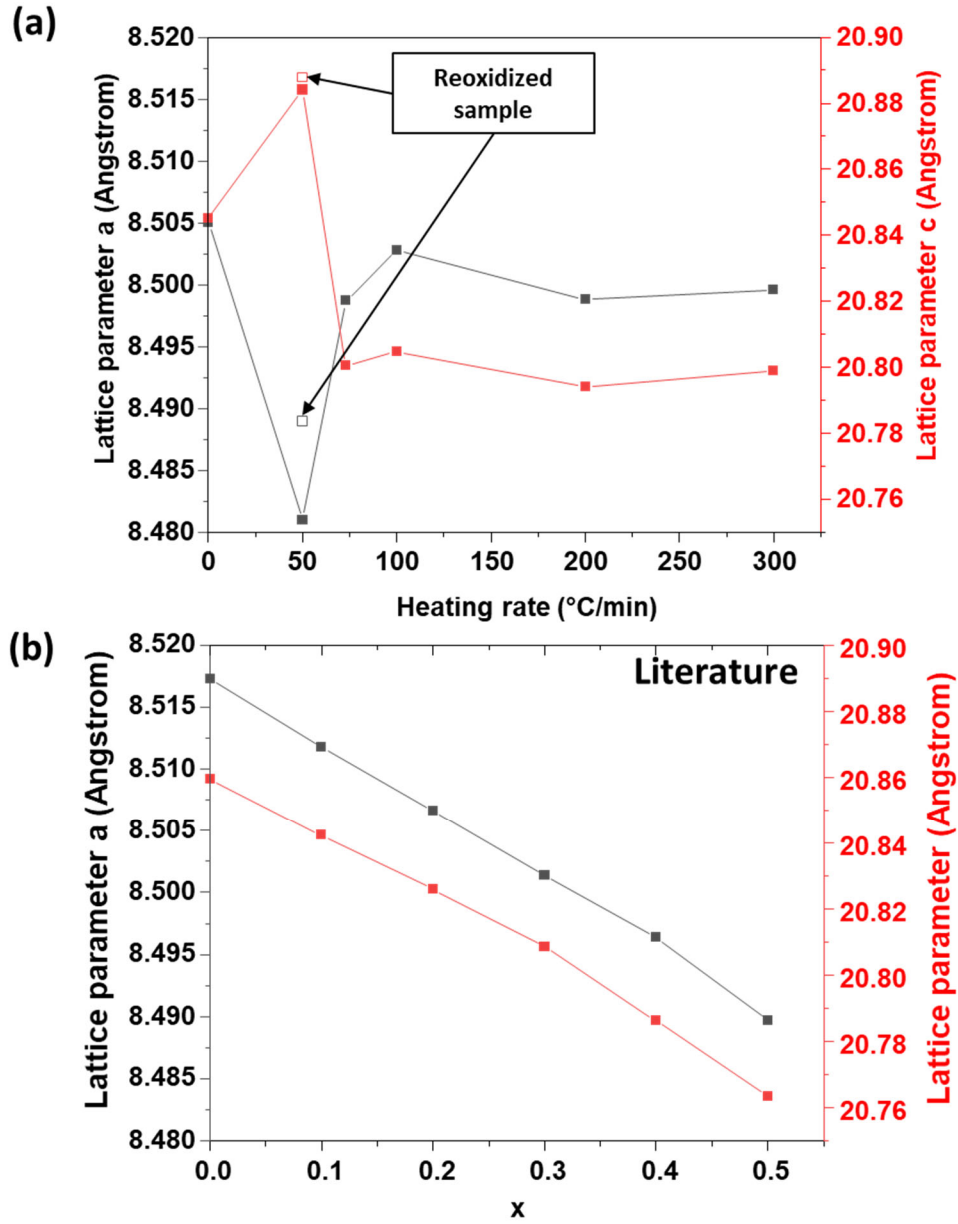


Figure S3: Evolution of the lattice parameters according to the heating rate applied during the SPS process (a) and lattice parameters evolution as function of the aluminium content inside the NASICON LATP structure, adapted from the reference <sup>1</sup>(b). The lines are given to guide the eyes.

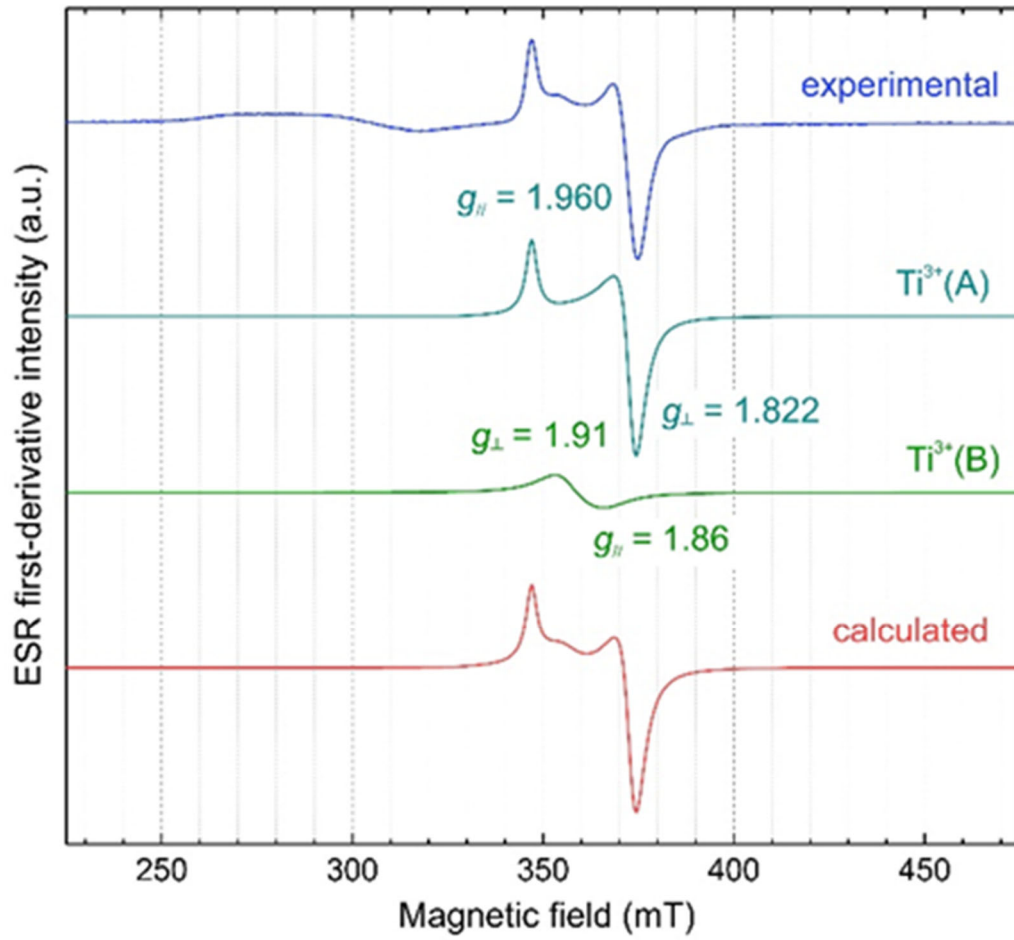


Figure S4 : Low temperature (30 K) X-band ESR powder spectra of sintered LTP (SPS 50°C/min) and simulated  $Ti^{3+}$  signals, and calculated spectrum (sum of  $Ti^{3+}(A)$  and  $Ti^{3+}(B)$  signals).

Table S2: Chemical shifts ( $\delta$ ), line widths (FWHM) and integrated intensities (II) of the different  $^{27}\text{Al}$  MAS NMR signals observed for the spectra collected for pristine LATP and samples sintered by SPS using heating rates of  $50^\circ\text{C}/\text{min}$  and  $200^\circ\text{C}/\text{min}$ .

Composition	$\text{AlO}_6$ (1)			$\text{AlO}_6$ (2)			$\text{AlO}_4$ ( $\text{AlPO}_4$ )			$\text{AlO}_4/\text{AlO}_6$ ratio
	Sample	$\delta$ (ppm)	FWHM	II [%]	$\delta$ (ppm)	FWHM	II [%]	$\delta$ (ppm)	FWHM	
Pristine LATP	-14.93	3.85	<b>30.5</b>	-17.5	11.09	<b>24.42</b>	38.03	6.57	<b>45.08</b>	<b>0.82</b>
SPS $50^\circ\text{C}/\text{min}$	-14.85	3.68	<b>55.94</b>	-17.73	8.64	<b>29.46</b>	38.48	5.15	<b>14.6</b>	<b>0.17</b>
SPS $200^\circ\text{C}/\text{min}$	-15.89	3.63	<b>73.95</b>	-18.24	7.43	<b>18.07</b>	38.02	5.63	<b>7.98</b>	<b>0.08</b>

The chemical formula proposed for LATP were determined as explained hereafter.

If we assumed that Al content is shared such as the material contains  $\{y \text{ mol AlPO}_4 \text{ for } 1 \text{ mol Li}_{1+x}\text{Al}_x\text{Ti}_{2-x}(\text{PO}_4)_3\}$ , the two Al-containing phases identified by XRD, and that we know in addition:

- (i) From NMR,  $y/x$
- (ii) From ICP analyses that  $(x+y)/(2-x) = 0.3/1.7$  or  $2x + 1.7y = 0.6$

It means that for:

- Pristine LATP:  $x = 0.18$  and  $y = 0.14$  and thus that the material is such as  $\{0.14 \text{ mol AlPO}_4 \text{ for } \text{Li}_{1.18}\text{Al}_{0.18}\text{Ti}_{1.82}(\text{PO}_4)_3\}$
- SPS  $50^\circ\text{C}/\text{min}$ :  $x = 0.26$  and  $y = 0.04$  and thus that the material is such as  $\{0.04 \text{ mol AlPO}_4 \text{ for } \text{Li}_{1.26}\text{Al}_{0.26}\text{Ti}_{1.74}(\text{PO}_4)_3\}$
- SPS  $200^\circ\text{C}/\text{min}$ :  $x = 0.281$  and  $y = 0.022$  and thus that the material is such as  $\{0.02 \text{ mol AlPO}_4 \text{ for } \text{Li}_{1.28}\text{Al}_{0.28}\text{Ti}_{1.72}(\text{PO}_4)_3\}$



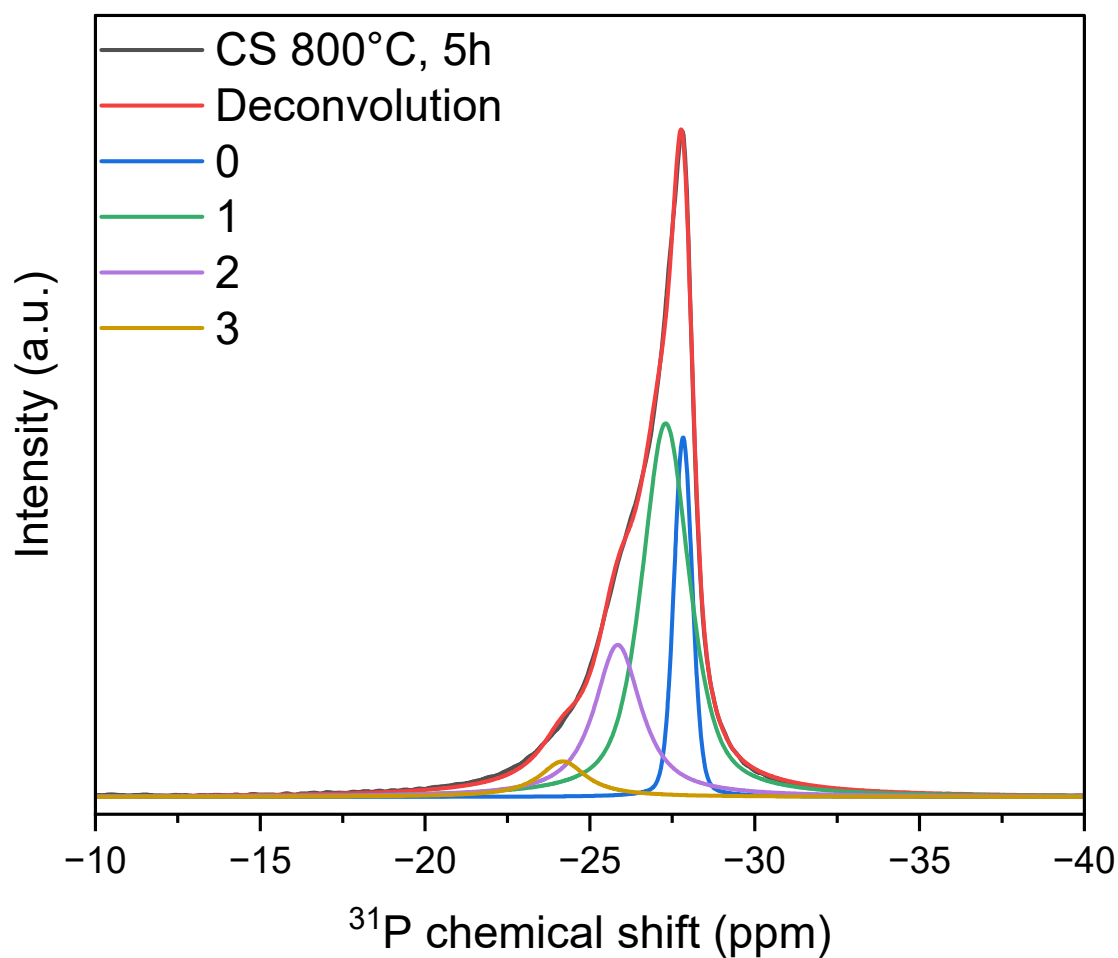


Figure S5: Fit of  $^{31}\text{P}$  MAS NMR spectrum collected for the sample sintered conventionally at 800°C during 5h. It is given as an example to highlight the complexity of the fitting. The attribution of each contribution was done based on Arbi et al. work<sup>2</sup>. The blue, green, purple and orange contributions are associated to  $\text{P}(\text{OTi})_4$ ,  $\text{P}(\text{OTi})_3(\text{OAl})_1$ ,  $\text{P}(\text{OTi})_2(\text{OAl})_2$  and  $\text{P}(\text{OTi})_1(\text{OAl})_3$  environments respectively. The one corresponding to  $\text{P}(\text{OAl})_4$  is obtained only for  $\text{Li}_{1-x}\text{Al}_x\text{Ti}_{2-x}(\text{PO}_4)_3$  compositions richer in Al ( $x > 0.3$ ).

Table S3: Chemical shifts ( $\delta$ ), line widths (FWHM) and integrated intensities (II) of the different  $^7\text{Li}$  MAS NMR signals observed for the spectra collected for pristine LATP, as well as samples sintered by SPS using heating rates of 50°C/min and 200°C/min.

Composition		Li1 LATP			Li3 LATP		
Sample	$\delta$ (ppm)	FWHM	II [%]	$\delta$ (ppm)	FWHM	II [%]	
Pristine LATP	-1.04	0.47	<b>75.15</b>	- 0.62	2.16	<b>24.85</b>	
SPS 50°C/min	-1.02	0.42	<b>54.5</b>	- 0.94	2.54	<b>45.5</b>	
SPS 200°C/min	-1.27	0.22	<b>48.64</b>	-1.18	0.25	<b>51.36</b>	

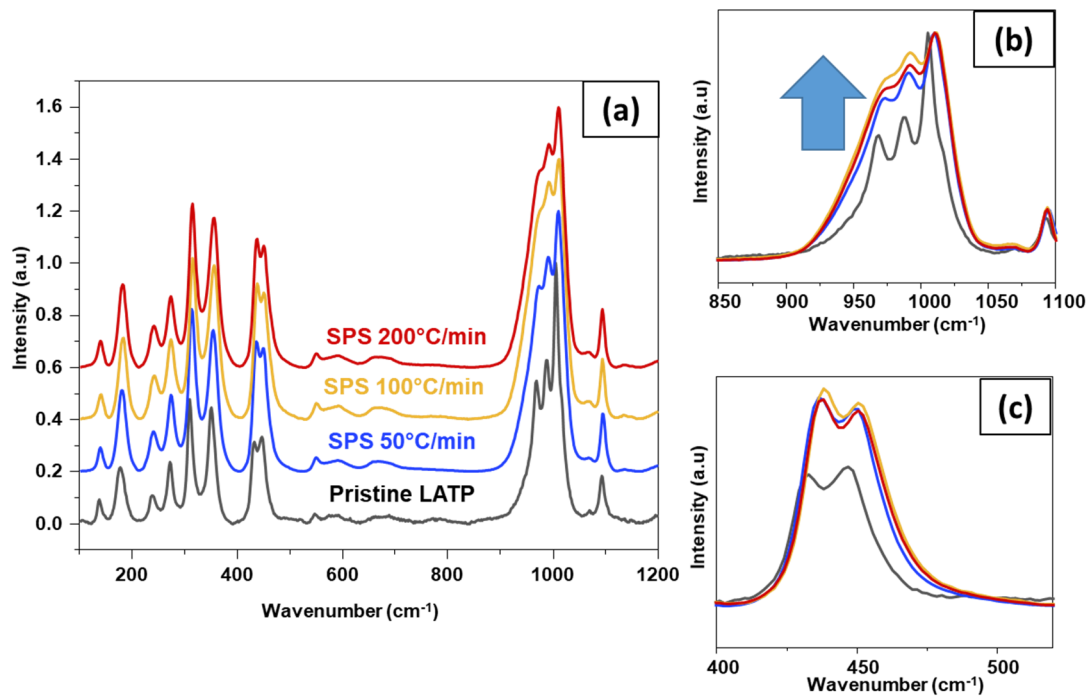


Figure S6 : Raman spectra of LATP pristine powder and samples sintered by SPS at heating rates of 50°C/min, 100°C/min and 200°C/min, obtained with a 532 nm laser in the range of 100 to 1200  $\text{cm}^{-1}$  with an acquisition time of 15 s and 160 accumulations. (b) and (c) are enlargements of the spectra given in (a), but set at the same background reference level.

This figure shows the comparison of the Raman spectra of the different samples studied: pristine LATP, and samples sintered by SPS at heating rates between 50°C/min and 200°C/min. The Raman modes have for all the samples similar shapes and same positions between 100  $\text{cm}^{-1}$  and 1200  $\text{cm}^{-1}$ . However, compared to those collected for the pristine LATP powder the Raman modes of the sintered samples are broader, suggesting an increasing content of  $\text{Al}^{3+}$  inside the NASICON framework. Indeed, Cretin et al.<sup>1</sup> have shown that the partial substitution of Al for Ti inside the NASICON structure involves a general enlargement of the Raman spectra due to distortion of the octahedral  $((\text{Ti}/\text{Al})\text{O}_6)$  and tetrahedral  $(\text{PO}_4)$  sites. The higher the heating rate during the sintering by SPS, the higher are the relative intensities of the  $\nu_1$  bands at 969 and 992  $\text{cm}^{-1}$  versus that of the  $\nu_3$  band at 1010  $\text{cm}^{-1}$ . This evolution is linked to the increase of Al content inside the structure, which induces local disordering around the  $\text{PO}_4^{3-}$  anions. The peaks at 438 and 450  $\text{cm}^{-1}$  can be ascribed to M-O symmetric bending motions ( $\nu_2$ ), whereas bands below 400  $\text{cm}^{-1}$  arise from external modes<sup>1-4</sup>.

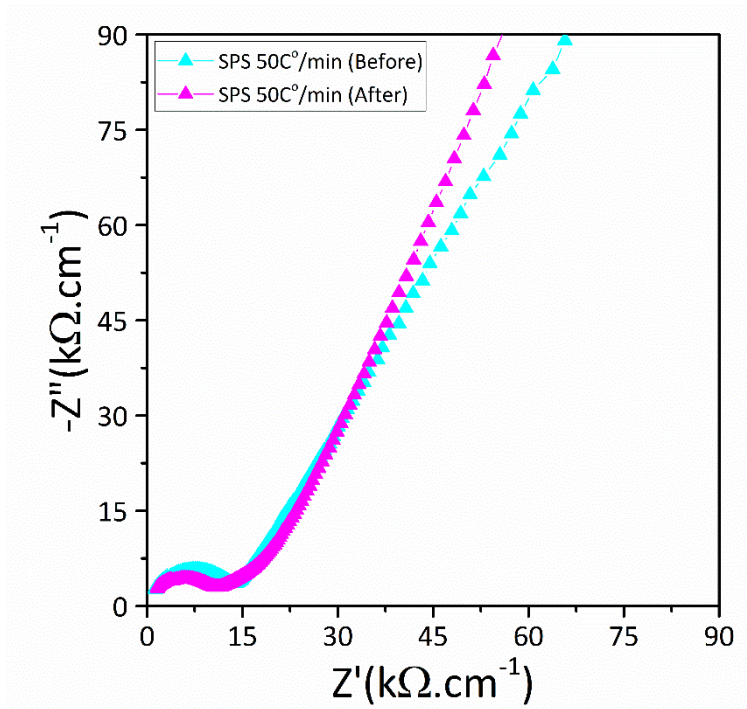


Figure S7: Impedance data collected at 25°C for LTP samples sintered by SPS at heating rate of 50°C/min before and after re-oxidation heat treatment (a). The complex impedance data shown here have been normalized regarding the shape factor of each sample for comparison purposes.

## References

1. Redhammer, G. J. *et al.* A single crystal X-ray and powder neutron diffraction study on NASICON-type  $\text{Li}_{1+x}\text{Ti}_{2-x}\text{Al}_x(\text{PO}_4)_3$  ( $0 \leq x \leq 0.5$ ) crystals: Implications on ionic conductivity. *Solid State Sciences* **60**, 99–107 (2016).
2. Arbi, K., Mandal, S., Rojo, J. M. & Sanz, J. Dependence of Ionic Conductivity on Composition of Fast Ionic Conductors  $\text{Li}_{1+x}\text{Ti}_{2-x}\text{Al}_x(\text{PO}_4)_3$ ,  $0 \leq x \leq 0.7$ . A Parallel NMR and Electric Impedance Study. *Chemistry of Materials* **14**, 1091–1097 (2002).
3. Burba, C. & Frech, R. Vibrational spectroscopic study of lithium intercalation into  $\text{LiTi}_2(\text{PO}_4)_3$ . *Solid State Ionics* **177**, 1489–1494 (2006).

4. Venkateswara Rao, A., Veeraiah, V., Prasada Rao, A. V., Kishore Babu, B. & Brahmayya, M. Spectroscopic characterization and conductivity of Sn-substituted  $\text{LiTi}_2(\text{PO}_4)_3$ . *Research on Chemical Intermediates* **41**, 4327–4337 (2015).
5. Cretin, M., Fabry, P. & Abello, L. Study of  $\text{Li}_1 + x\text{Al}_x\text{Ti}_2 - x(\text{PO}_4)_3$  for  $\text{Li}^+$  potentiometric sensors. *Journal of the European Ceramic Society* **15**, 1149–1156 (1995).
6. Giarola, M. *et al.* Structure and Vibrational Dynamics of NASICON-Type  $\text{LiTi}_2(\text{PO}_4)_3$ . *The Journal of Physical Chemistry C* **121**, 3697–3706 (2017).